ISS2012

BaFe$_2$As$_2$/Fe bilayers with [001]-tilt grain boundary on MgO and SrTiO$_3$ bicrystal substrates

K. Iida[a*], S. Haindl[b], F. Kurth[a], J. Hänisch[a], L. Schulz[a], B. Holzapfel[a]

[a]*Institute for Metallic Materials, IFW Dresden. 01171 Dresden, Germany*
[b]*Institute for Solid State Research, IFW Dresden. 01171 Dresden, Germany*

Abstract

Co-doped BaFe$_2$As$_2$ (Ba-122) can be realized on both MgO and SrTiO$_3$ bicrystal substrates with [001]-tilt grain boundary by employing Fe buffer layers. However, an additional spinel (i.e. MgAl$_2$O$_4$) buffer between Fe and SrTiO$_3$ is necessary since an epitaxial, smooth surface of Fe layer can not be grown on bare SrTiO$_3$. Both types of bicrystal films show good crystalline quality.

Keywords: Pnictide; Grain boundary; Thin film; Bicrystal; Buffer layer

1. Introduction

In high-T_c cuprates, [001]-tilt grain boundaries (GBs) in MgO and SrTiO$_3$ bicrystal substrates have been commonly used for realizing Josephson junctions as well as investigating transport properties of GBs. After the discovery of Fe-based pnictide superconductors,[1] the community became immediately interested in exploring grain boundaries in this new class of superconductors.

Despite the recent success of realizing Co-doped BaFe$_2$As$_2$ (Ba-122) on [001]-tilt GB MgO and SrTiO$_3$ bicrystal substrates,[2-3] these substrates may not be suitable for several reasons. Firstly, a large misfit between Ba-122 and MgO of around 6 % leads to low crystalline quality or even non-epitaxial growth under our deposition condition.[4] Secondly, the SrTiO$_3$ substrate becomes electrically conductive under ultra-high vacuum (UHV) conditions, which may compromise transport measurements particularly near the normal-superconducting transition. However, implementation of Fe for MgO and Fe+MgAl$_2$O$_4$ for SrTiO$_3$ as buffer layers can solve those problems. An Fe layer itself is electrically conductive, however, the recalculation of the superconducting transition temperature (T_c) and the critical current density (J_c) is possible due to its thin layer thickness (20 nm).[5] In this report, the fabrication of Co-doped Ba-122 thin films on both [001]-tilt bicrystal MgO and SrTiO$_3$ substrates and their transport properties are presented in detail. For the aim of bicrystal Josephson junctions, substrates with a large [001]-tilt angle of over 20° have been used in this investigation.

2. Experimental procedure

* Corresponding author. Tel.:+49-351-4659-608; fax: +49-351-4659-541.
E-mail address: k.iida@ifw-dresden.de

2.1. Ba-122 on [001]-tilt MgO bicrystal

A 20 nm thick Fe buffer layer was deposited by means of pulse laser deposition (PLD) on a [001]-tilt MgO bicrystal substrate with misorientation angle of θ_{GB}=36.8° (nominal value) at room temperature, followed by a high-temperature annealing at 700°C. This process is very effective for obtaining epitaxial Fe layers with flat surface. After the Fe buffer preparation, Co-doped Ba-122 ($BaFe_{1.8}Co_{0.2}As_2$) with 100 nm thickness was deposited at 700 °C. All deposition processes have been conducted under UHV condition. A detailed description of both Fe buffer and Co-doped Ba-122 deposition procedure can be found in Ref. [6]. After the structural characterization described in sub-section *2.3*, Au layers were deposited on the films by PLD at room temperature followed by ion beam etching to fabricate bridges of 0.5 mm width and 1 mm length for transport measurements.

2.2. Ba-122 on [001]-tilt SrTiO₃ bicrystal

A $MgAl_2O_4$ buffer was deposited on a [001]-tilt GB SrTiO₃ bicrystal substrate with θ_{GB} = 30° at 650 °C by PLD in UHV condition (pulse number 4000 at 40 mJ). In a pilot experiment, we have confirmed that $MgAl_2O_4$ can be grown epitaxially on SrTiO₃ (100) substrate. After the primary buffer deposition, the $MgAl_2O_4$-buffered SrTiO₃ substrate was cooled to room temperature for the secondary, Fe buffer deposition. A 20 nm thick Fe buffer was prepared by the same procedure as described in sub-section *2.1* except for the annealing temperature. Here, a slightly higher temperature of 750°C was employed. After the Fe buffer preparation, a 100 nm thick Co-doped Ba-122 ($BaFe_{1.84}Co_{0.16}As_2$) layer was deposited. *In-situ* gold layer deposition at room temperature was conducted after the Ba-122 deposition for the aim of protection from possible damage during the structuring process.

2.3. Structural characterization and transport measurements

Phase purity and out-of-plane texture were investigated by means of X-ray diffraction in Bragg-Brentano geometry with Co-K$_\alpha$ radiation. In-plane orientation of both Fe and Co-doped Ba-122 were investigated by using the 110 and 103 poles, respectively, in a texture goniometer operating with Cu-K$_\alpha$ radiation. The respective measured reflection of the MgO and SrTiO₃ bicrystal substrates for in-plane texture measurements are 220 and 110.

Superconducting properties were measured in a Physical Property Measurement System (PPMS, Quantum Design) by a standard four-probe method with a criterion of 1 $_\mu$ Vcm^{-1} for evaluating J_c.

3. Results and discussion

XRD patterns in logarithmic scale (fig. 1 (a)) clearly show that the film has been grown with high phase purity and *c*-axis texture, i.e. with [001] perpendicular to the substrate surface. Fig. 1 (b) shows the φ-scans of the 103 Ba-122, the 110 Fe and the 220 MgO. It is evident from fig. 1 (b) that two grains with θ_{GB}~37.1°, which is slightly larger than the nominal value of 36.8°, are grown due to the perfect transfer of the grain orientation from the substrate via Fe buffer to the Ba-122 layer. Here the respective average $\Delta\phi_{Ba-122}$ and $\Delta\phi_{Fe}$ are 0.84° and 0.80° (not corrected for instrumental broadening), indicative of good in-plane alignment for both layers. The GB is symmetric, i.e. it is situated with $\theta_{GB}/2$ to (100) in both grains.
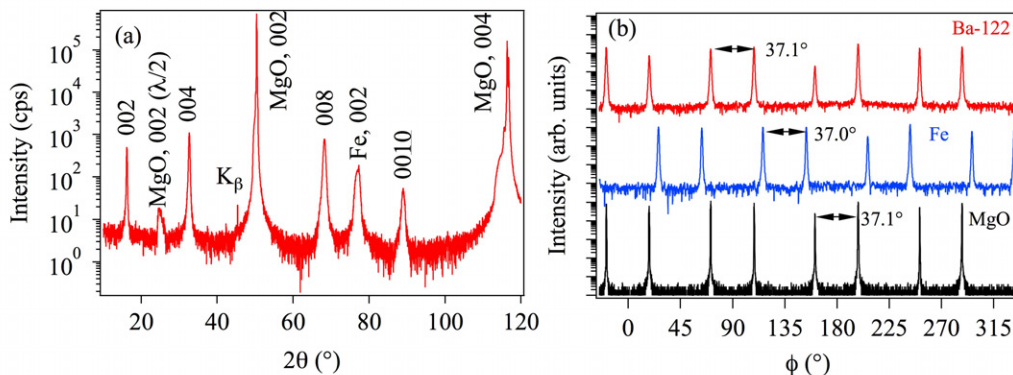

Fig. 1. (a) The θ/2θ scan of Ba-122/Fe bilayer on [001]-tilt GB MgO bicrystal substrate in Bragg- Brentano geometry using Co-Kα radiation. (b) The φ-scans of the 103 Ba-122, the 110 Fe and the 220 MgO. Average misorientation angles are 37.1°, 37.0°, and 37.1° for Ba-122, Fe and MgO, respectively.

R-T curves in fig. 2 (a) show that both the inter- and intra-grain bridge have the same onset T_c as well as zero resistance, indicating the high quality of the bicrystal films. The field dependence of $J_c(B\|c)$ for both the inter- and intra-grain bridge at various temperatures is displayed in fig. 2 (b). Clearly, the intra-grain J_c (J_c^{intra}) is higher than the inter-grain J_c (J_c^{inter}) at low magnetic fields regime due to the large θ_{GB}. The difference between J_c^{intra} and J_c^{inter} is getting smaller with increasing applied field and finally both curves overlap at the irreversibility field for $\theta_{GB} \sim 37°$. On the assumption that the weak-link behavior is empirically described by $J_c^{inter}=J_c^{intra}\exp(-\theta_{GB}/\theta_0)$ in low field regime, the characteristic angle (θ_0) is estimated to around 7.9° for our Co-doped Ba-122 bicrystal films (fig.2 (c)), which is almost twice as large as that of $YBa_2Cu_3O_7$ [7].
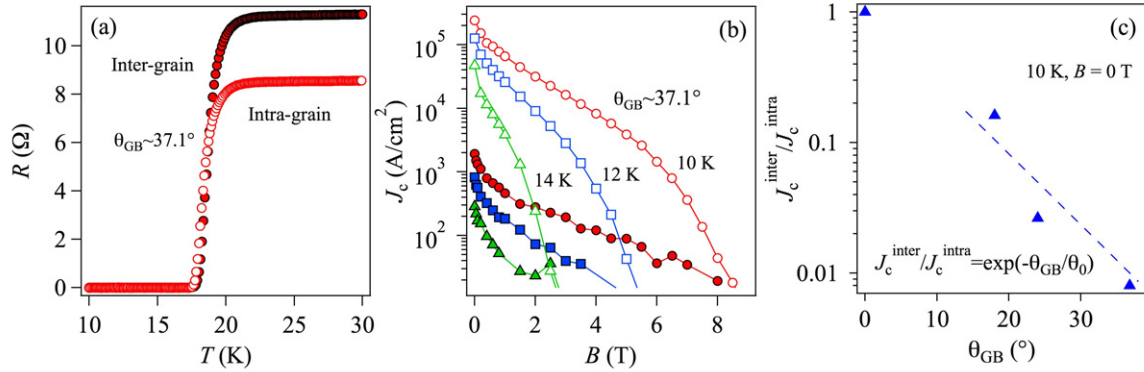

Fig. 2. (a) *R-T* curves of inter- and intra-grains. Both curves show the same T_c of around 20 K. (b) J_c-*B* performances ($B\|c$) of the corresponding grains at different temperatures. Open symbols represent the intra-grain and the solid symbols show the inter-grain curves. (c) Normalized critical current density (J_c^{inter}/J_c^{intra}) as a function of θ_{GB} at 10 K.

The growth of epitaxial Fe with smooth surface on $SrTiO_3$ substrate is not straightforward, which is presumably due to the difference in crystal structure rather than to the lattice mismatch. As a result, epitaxial growth of Ba-122 is hardly achieved on Fe-buffered $SrTiO_3$. Indeed, fiber textured Fe is observed (fig. 3 (a)), when it is prepared directly on $SrTiO_3$ substrate with the same procedure as on MgO substrates. In order to avoid this problem, an additional buffer layer of $MgAl_2O_4$ between Fe and $SrTiO_3$ substrate has been used. $MgAl_2O_4$ fits better to accommodate the lattice mismatch to Fe rather than MgO as shown in Table 1. Here, the lattice mismatch is defined as $(a_f-a_s)/a_f$, where a_f and a_s are the lattice parameters of Fe and substrates, respectively. Additionally, a small lattice mismatch of 3.4 % between $MgAl_2O_4$ and $SrTiO_3$ may lead to good epitaxial growth of the $MgAl_2O_4$ buffer.

Fig. 3 (b) shows the 110 pole figure of Fe on $MgAl_2O_4$-buffered $SrTiO_3$ fabricated by the same procedure described in sub-section *2.1*. It is clear from fig. 3 (b) that a perfect textured growth of Fe is realized (average $\Delta\phi_{Fe}$=0.61°). During heating of Fe, evolution of the Fe-layer texture was observed through reflection high energy electron diffraction (RHEED), which is a similar observation of Fe on single crystalline MgO substrates.[8] The RHEED images of the Fe layer on $MgAl_2O_4$-buffered $SrTiO_3$ after the high temperature annealing showed only streak patterns, indicative of surface smoothing. This architecture also prevents the current-shunting effect between $SrTiO_3$ and Co-doped Ba-122. This buffer architecture offers the opportunity to grow smooth epitaxial Fe layers on various perovskite substrate such as $(La,Sr)(Al,Ta)O_3(100)$ substrate (not shown in this paper).
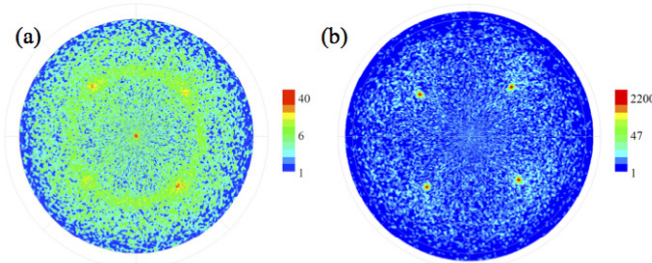

Fig. 3. (a) The 110 pole figure measurement of Fe on bare $SrTiO_3$ and (b) $MgAl_2O_4$-buffered $SrTiO_3$.

Table 1. The crystal structure, lattice parameter and the lattice mismatch to Fe of MgO and $MgAl_2O_4$.

Materials	Crystal structure	Lattice parameter (nm)	Lattice mismatch (%)
MgO	Rock salt	0.421	3.7
$MgAl_2O_4$	Spinel	0.8083 (a/2=0.4042)	-0.4

Structural characterization of Ba-122/Fe/$MgAl_2O_4$ on [001]-tilt GB $SrTiO_3$ substrate by means of X-ray diffraction is summarized in figs. 4. As stated earlier, *in-situ* Au layer deposition was conducted after the Ba-122 deposition, which explains the 111 reflection of Au in fig. 4 (a). It is further clear from fig. 4 (a) that only 00l reflections of Ba-122 with a small amount of the 110 reflection are observed. Fig. 4 (b) displays the ϕ-scans of the 103 Ba-122, the 110 Fe and the 110 $SrTiO_3$. Clear 8 peaks from two grains with a rotational angle of 30° are apparent. Accordingly, an epitaxial Ba-122 film is formed on [001]-tilt $SrTiO_3$ bicrystal substrate. The onset T_c = 24 K of the film is almost identical to that of Ba-122/Fe bilayers on single crystal substrates. (fig. 4 (c)) This value is higher than the intra-grain T_c deposited on MgO bicrystal presented in fig. 2 (a) due to a higher deposition temperature as well as different PLD targets (i.e. different Co concentration). The resultant bicrystal junctions show clear Josephson effects and the detailed studies can be found in Ref. [9].
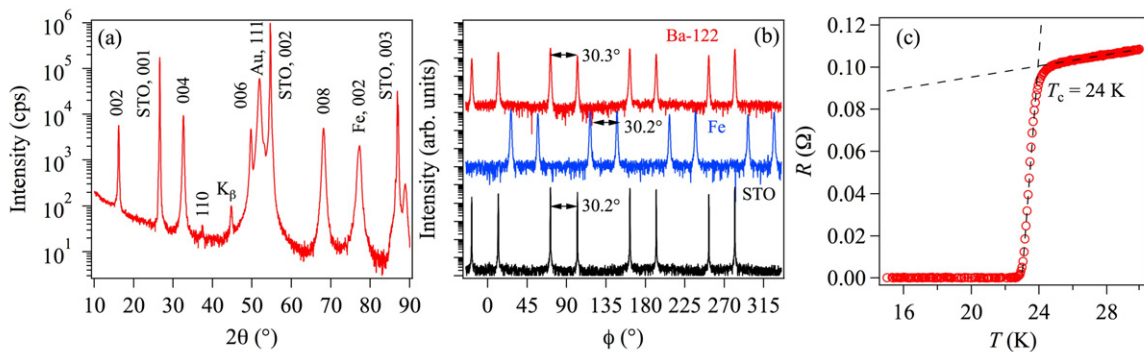

Fig. 4. (a) The $\theta/2\theta$ scan of Ba-122/Fe/$MgAl_2O_4$ trilayer on [001]-tilt $SrTiO_3$ (STO) bicrystal substrate in Bragg- Brentano geometry using Co-Kα radiation. (b) The ϕ-scans of the 103 Ba-122, the 110 Fe, and 110 STO. Average misorientation angles are 30.3°, 30.2°, and 30.2° for Ba-122, Fe and STO, respectively. (c) Intra-grain T_c was recorded as 24 K.

4. Summary

High-quality Co-doped Ba-122 bicrystal films can be realized on both [001]-tilt MgO and $SrTiO_3$ substrates by employing Fe buffer layers via pulsed laser deposition. The additional $MgAl_2O_4$ buffer between Fe and $SrTiO_3$ is necessary for realizing epitaxial Ba-122. The characteristic angle of Co-doped Ba-122 in low field regime is about 8°, which is almost twice as large as that of $YBa_2Cu_3O_7$.

Acknowledgements

References

[1] Y. Kamihara, T. Watanabe, M. Hirano, H. Hosono, J. Am. Chem. Soc. 130 (2008) 3296.
[2] S. Lee, J. Jiang, J.D. Weiss, C.M. Folkman, C.W. Bark, C. Tarantini *et al*., Appl. Phys. Lett. 95 (2009) 212505.
[3] T. Katase, Y. Ishimaru, A. Tsukamoto, H. Hiramatsu, T. Kamiya, K. Tanabe, H. Hosono, Nat. Commun. 2 (2011) 409.
[4] T. Thersleff, K. Iida, S. Haindl, M. Kidszun, D. Pohl, A. Hartmann *et al*., Appl. Phys. Lett. 97 (2010) 022506.
[5] S. Trommler, R. Hühne, J. Hänisch, E. Reich, K. Iida, S. Haindl *et al*., Appl. Phys. Lett. 100 (2012) 122602.
[6] K. Iida, S. Haindl, T. Thersleff, J. Hänisch, F. Kurth, M. Kidszun *et al*., Appl. Phys. Lett. 97 (2010) 172507.
[7] H. Hilgenkamp, J. Mannhart, Rev. Mod. Phys. 74 (2002) 485.
[8] K. Iida, J Hänisch, S. Trommler, S. Haindl, F. Kurth, R. Hühne *et al*., Supercond. Sci. Technol. 24 (2011) 125009.
[9] S. Schmidt, S. Döring, F. Schmidl, V. Tympel, S. Haindl, K. Iida *et al*., IEEE Trans. Appl. Supercond. 23 (2013) 7300104.